

High Performance Single Layered WSe₂ *p*-FETs with Chemically Doped Contacts

Hui Fang^{1,2,3}, Steven Chuang^{1,2,3}, Ting Chia Chang¹, Kuniharu Takei^{1,2,3}, Toshitake Takahashi^{1,2,3}, and Ali Javey^{1,2,3,*}

¹Electrical Engineering and Computer Sciences, University of California, Berkeley, CA, 94720.

²Materials Sciences Division, Lawrence Berkeley National Laboratory, Berkeley, CA 94720.

³Berkeley Sensor and Actuator Center, University of California, Berkeley, CA, 94720.

* Correspondence should be addressed to A.J. (ajavey@eecs.berkeley.edu).

Abstract - We report high performance *p*-type field-effect transistors based on single layered (thickness, ~0.7 nm) WSe₂ as the active channel with chemically doped source/drain contacts and high- κ gate dielectrics. The top-gated monolayer transistors exhibit a high effective hole mobility of ~250 cm²/Vs, perfect subthreshold swing of ~60 mV/dec, and I_{ON}/I_{OFF} of >10⁶ at room temperature. Special attention is given to lowering the contact resistance for hole injection by using high work function Pd contacts along with degenerate surface doping of the contacts by patterned NO₂ chemisorption on WSe₂. The results here present a promising material system and device architecture for *p*-type monolayer transistors with excellent characteristics.

Keywords - WSe₂, monolayer, FETs, surface chemical doping, two-dimensional, chalcogenide layered semiconductors

Exploratory research is needed to develop materials, structures, and device technologies for future sub-5 nm gate length field-effect transistors (FETs). At such small scales, severe short channel effects limit the performance and operation of electronic devices¹. Theoretical studies have shown that the use of large band gap semiconductors with ultrathin bodies and/or gate-all around structures are essential to minimize the short channel effects at extreme scaling limits¹. Specifically, for ultrathin body devices, a general guideline dictates a body thickness of $< 1/3$ of the gate length for effective electrostatic control of the channel by the gate electrode³. For sub-5 nm gate lengths, this corresponds to channel materials with only 1-2 atomic layers in thickness. In this regard, single layered semiconductors are excellent candidates for the channel material of future monolayer-FETs (ML-FETs). As compared to materials with diamond/zinc-blende structure, layered semiconductors exhibit advantageous surfaces with minimal roughness, dangling bonds, defect states and native oxides. Among various layered materials, graphene has achieved worldwide interest and numerous interesting applications have been proposed^{4,5,6,7}. However, graphene does not have an intrinsic band gap, which severely limits its digital logic applications. Meanwhile, the band gap of graphene nanoribbons shown to date is still too small for ultrashort channel FETs⁸. Recent advances in monolayer and few layered MoS₂, a chalcogenide semiconductor with a large band gap of $E_g \sim 1.8$ eV, has shown the potential use of layered semiconductors for high performance *n*-type FETs (*n*-FETs)⁹. To date, however, high mobility monolayer *p*-FETs with high I_{ON}/I_{OFF} have not been reported, and more importantly routes for controllable doping of chalcogenide layered semiconductors at the source/drain (S/D) contacts for low parasitic resistances have not been explored. In this report, by developing a surface dopant-profiling technique, we demonstrate the first high hole mobility WSe₂ ML-FETs (body thickness of ~ 0.7 nm) with degenerately doped contacts. The use of heavily p-doped

contacts is essential in lowering the metal contact resistances to WSe₂ by orders of magnitude, and enabling the demonstration of *p*-FETs with peak effective mobility of ~250 cm²/Vs, near ideal subthreshold swing (SS) of ~60 mV/decade, and high I_{ON}/I_{OFF} of >10⁶.

WSe₂ is a layered semiconductor with a bulk indirect bandgap of ~1.2 eV (ref. 10-11). A recent study of bulk WSe₂ FETs revealed an intrinsic hole mobility of up to 500 cm²/Vs (ref. 12). However, the bulk devices exhibited poor I_{ON}/I_{OFF} ratio of less than 10 at room temperature, along with ambipolar behavior, both of which are highly undesirable for digital logic applications. This is presumably due to the use of a bulk (i.e., thick) body which results in large OFF state leakage currents. Here we applied the well-known mechanical exfoliation method to obtain a single layer of WSe₂ from a bulk crystal (Nanoscience Instruments, Inc) on Si/SiO₂ substrates for ML-FET fabrication and characterization. Fig. 1a shows an optical microscope image of a single layer WSe₂ flake (light orange) transferred on top of a Si/SiO₂ (thickness, 270 nm) substrate. This thickness of SiO₂ is optimized to optically visualize the contrast of single layer and few layer WSe₂, similar to the cases of graphene and MoS₂ (ref. 9). Fig. 1b depicts the atomic force microscope (AFM) image of a single layered WSe₂ flake, with Fig. 1c showing the lateral height profile at the edge of the flake. From AFM measurements, the thickness of the single layer is determined to be ~0.7 nm, which agrees with the crystallography data of WSe₂ in literature¹³. Note that the surface roughness of WSe₂ is similar to the Si/SiO₂ background, indicating that the layer is uniform and the surface roughness is minimal, which is essential for obtaining high carrier mobilities with low surface roughness scattering rates.

Large E_g semiconductors such as WSe₂ are notoriously known for their difficulty in forming ohmic metal contacts. Therefore, it is important to shed light on the metal-WSe₂ Schottky barriers (SBs), and explore routes towards minimizing the contact resistances to enable

exploration of intrinsic material and device properties. In this regard, we have explored different metal source/drain (S/D) contacts, including Pd, Ag, Ni, Au, Ti and Gd for back-gated WSe₂ FETs. The fabrication process involves the transfer of WSe₂ layers onto a Si/SiO₂ substrate, followed by a 1hr acetone bath to remove the tape residues, S/D metal contact patterning by lithography, evaporation and lift off processes. Here the S/D length is fixed at $L \sim 8 \mu\text{m}$. Based on the various metal contacts explored, high work function Pd was found to form the lowest resistance contact to the valence band of WSe₂ for hole transport, with devices exhibiting the highest unit-width normalized ON currents. As depicted in the back-gated transfer characteristics (Fig. 2a), Pd contacted FETs exhibit clear p-type conduction, without ambipolar transport. In contrast, lower work function metal contacts resulted in FETs that conduct in both n and p regimes with low current levels, reflecting high SB heights to both conduction and valence bands of WSe₂. Specifically, Ti forms near mid-gap SBs to WSe₂ with low-current ambipolar characteristics (Fig. 2a-b). The results here highlight the importance of selecting high work function metals with good interfaces to WSe₂ in order to lower the SB height at the contacts for hole transport. Clearly, Fermi level pinning is weak or non-existent at metal-WSe₂ interfaces. Further investigation of the exact effect of the metal work function and interface chemistry on the barrier height is needed in the future.

Although Pd was found to form the best contact for hole transport among the various metals explored, a small SB may still exist at the Pd-WSe₂ interface given the large E_g of WSe₂. To shed light on the contact properties of Pd, surface hole doping of WSe₂ was explored. By heavily *p*-doping WSe₂, the width of any barriers at the metal interfaces can be drastically reduced, resulting in more efficient tunneling of the carriers and lower resistance contacts. Inspired by the surface doping approach in carbon nanotubes and graphene^{14,15,16}, here we

utilized NO₂ molecules as a *p*-type surface dopant. NO₂ molecules are expected to be absorbed both physically and chemically on top of the WSe₂ surface as illustrated in Fig. 3a. Due to the strong oxidizing property of NO₂, the molecules act as “electron pumps” when chemisorbed to WSe₂. Fig. 3b shows the transfer characteristics of a back-gated WSe₂ ML-FET before and after NO₂ exposure. The device was exposed to 0.05% NO₂ in N₂ gas for 10 min, beyond which the doping effect was found to saturate presumably due to the NO₂ saturation coverage on the surface¹⁴. Here, the entire channel is exposed to NO₂, resulting in blanked (i.e., unpatterned) doping of WSe₂. The weak gate-voltage dependence of current after NO₂ exposure clearly reflects that WSe₂ is heavily doped (Fig. 3b). Moreover, the current at high negative V_{GS} (ON state) is enhanced by >1000x after NO₂ doping, which can be attributed to the lowering of contact resistance by thinning the Pd-WSe₂ SB width for hole injection. In addition, NO₂ may increase the work function of Pd, thereby lowering the SB height at the interface. This work function increase is possibly due to the formation of surface/subsurface metastable palladium oxides when NO₂ is absorbed on Pd as previously reported in literature^{17,18}.

To estimate the 2-D sheet carrier density (n_{2D}) of WSe₂ after NO₂ doping, the source/drain current (I_{DS}) at zero gate voltage was modeled as $I_{DS} = q \cdot n_{2D} \cdot W \cdot \mu \cdot V_{DS} / L$, where q is the electron charge, W and L are the width and length of channel, respectively, μ is the field-effect mobility ($\sim 140 \text{ cm}^2/\text{Vs}$ as extracted from the I_{DS} - V_{GS} transfer characteristic), and V_{DS} is the source/drain voltage. Since the channel shape is often irregular, the width is defined as the total channel area divided by the length. We note that the field-effect mobility from back-gated WSe₂ ML-FETs doped with NO₂ is 1-2 orders of magnitude higher than MoS₂ ML-FETs without the high- κ dielectric mobility booster⁹. This could be either due to the different surface characteristics of WSe₂ as compared to MoS₂ and/or due to the lower contact resistance observed

here by doping the contacts. n_{2D} is extracted to be $\sim 2.2 \times 10^{12} \text{ cm}^{-2}$, which corresponds to a doping concentration of $\sim 3.1 \times 10^{19} \text{ cm}^{-3}$. At this doping concentration, Fermi level lies at $\sim 16 \text{ meV}$ below the valence band edge (E_V), as calculated from the Joyce-Dixon Approximation¹⁹ and an effective hole density of state of $N_V = 2.54 \times 10^{19} \text{ cm}^{-3}$ (ref. 20). Therefore, NO_2 exposed WSe_2 layers are degenerately doped. This doping level, however, is lower than the NO_2 surface monolayer density of $\sim 1.4 \times 10^{15} \text{ cm}^{-2}$ (assuming a perfect monolayer coverage)¹⁷, suggesting that on average ~ 0.001 electron is transferred per NO_2 molecule. It should be noted that NO_2 doping is reversible due to the gradual desorption of NO_2 molecules from the WSe_2 surface once exposed to ambient air (Fig. S1). In the future, other dopant species and/or process schemes should be explored for permanent doping.

Next, we explored patterned p -doping of WSe_2 for the fabrication of top-gated ML-FETs with self-aligned, chemically doped S/D contacts. Pd/Au (30/20 nm) metal contacts were first defined by lithography and metallization. Gate electrodes, underlapping the S/D by a distance of 300 - 500 nm were then patterned by e-beam lithography and using PMMA as resist, followed by atomic layer deposition (ALD, at 120°C) of 17.5 nm ZrO_2 as the gate dielectric, the deposition of Pd metal gate, and finally lift-off of the entire gate stack in acetone. While it has been reported that direct ALD on pristine graphene is not possible due to the lack of dangling bonds, uniform ALD of Al_2O_3 and HfO_2 on MoS_2 at the optimized temperature window has been previously demonstrated and attributed to the physical absorption of precursors on the basal plane^{21,22}, which we assume also applies to WSe_2 . The devices are then exposed to a NO_2 environment and measured. Fig. 4a shows the schematic illustration of a top-gated ML-FET after NO_2 S/D doping. The exposed (underlapped) regions are p -doped heavily, while the gated region remains near intrinsic due to the protection of the active channel by the gate stack. This $p+i/p+$ device

structure is similar to conventional ultra-thin body Si MOSFETs. Fig. 4b shows the transfer characteristics of a ~ 9.4 μm channel length WSe₂ ML-FET (see Fig. S2 for the device optical images) before and after NO₂ contact doping. Here the back-gate voltage is fixed at -40 V to electrostatically dope the underlapped regions for both before and after NO₂ exposure. As a result, the difference in the current-voltage characteristics for the two measurements purely arises from the change of the metal-WSe₂ contact resistance, rather than the resistance of the underlapped regions. As depicted in Fig. 4b, a drastic enhancement of $\sim 1000\times$ improvement in the ON current is observed in the device after surface doping of the contacts by NO₂, without a change in I_{OFF} . A small shift in the threshold voltage to the positive direction is observed after NO₂ contact doping, which could be due to the increase of the Pd metal gate work function by NO₂. The ML-FET with doped contacts exhibits an impressive $I_{\text{ON}}/I_{\text{OFF}}$ of $>10^6$ arising from the large band-gap of WSe₂ combined with the monolayer-thick body which minimizes OFF state leakage currents.

Importantly, the transfer characteristics at room temperature shows a perfect subthreshold swing (SS), reaching the theoretical limit of $\ln(10) \times kT/q = 60$ mV/dec for a MOSFET, which originates from the thermionic emission of the source holes with density of states (DOS) tailed by the Fermi-Dirac distribution. For an experimental (i.e., non-ideal) MOSFET, SS is given as $\eta \times 60$ mV/decade, where $\eta \approx 1 + \frac{C_{it}}{C_{ox}}$ is the body factor, and C_{it} is the capacitance caused by the interface traps ($C_{it} = D_{it} \cdot q^2$, with D_{it} being the interface trap density) and $C_{ox} = \epsilon_{ox} \epsilon_0 / T_{ox}$ is the top gate oxide capacitance per unit area ($\epsilon_{ox} \sim 12.5$ is the dielectric constant of ZrO₂, ϵ_0 is the vacuum permittivity, and $T_{ox} = 17.5$ nm is the ZrO₂ thickness). The experimental SS ~ 60 mV/decade for WSe₂ ML-FETs suggests the near unity η caused by $C_{it} \ll C_{ox}$. The low C_{it} is

attributed to the lack of surface dangling bonds for layered semiconductors. Notably our measured SS outperforms all Ge and III-V MOSFETs, firmly indicating that WSe₂ has optimal switching characteristics for low power and high speed electronics.

Next the effective hole mobility, μ_{eff} , of top-gated WSe₂ ML-FETs with doped contacts was extracted from the I-V characteristics by using the relation,

$$\mu_{eff} = \frac{\partial I_{DS}}{\partial V_{DS}} \frac{L_G}{C_{ox}(V_{GS} - V_T - 0.5V_{DS})},$$

where V_T is the threshold voltage and L_G is the gate length.

The long-channel device exhibits a peak hole effective mobility of ~ 250 cm²/Vs (Fig. 4c). The mobility does not degrade severely at high fields (Fig. 4c), which should be attributed to the fact that the carriers are already close to the gate in a single layered channel, and that surface roughness is minimal. Therefore, the gate oxide thickness can be further scaled without severe mobility degradation, again indicating that WSe₂ is a promising candidate for future scaled electronics. It must be noted that the channel is one monolayer thick (~ 0.7 nm), significantly thinner than the previously reported high hole mobility III-V or Ge MOSFETs, even in ultrathin body (UTB) configuration. For conventional diamond/zinc-blende structured material channels, severe mobility degradation occurs when reducing the channel thickness due to the enhanced scattering from both surface roughness and dangling bonds. For example, the peak effective hole mobility of strained-InGaSb based UTB-FETs drops from ~ 820 to 480 cm²/Vs when the body thickness is reduced from 15 nm to 7 nm²³. Therefore, the measured mobility of 250 cm²/Vs for our monolayer-thick WSe₂ FETs is impressive.

The output characteristic of the same top gated WSe₂ ML-FET with doped contacts is shown in Fig. 4d. The long-channel device exhibits clear current saturation at high V_{DS} due to pinch-off, similar to the conventional MOSFETs. In the low V_{DS} regime, the I-V curves are

linear, depicting the ohmic metal contacts. Overall, the results here demonstrate the potential of WSe₂ monolayers along with the essential patterned doping of the contacts for high performance *p*-FETs.

In conclusion, the layered semiconductor WSe₂, has been thinned down to a single layer through mechanical exfoliation and fabricated into *p*-FETs with promising hole mobility and perfect subthreshold characteristics. A NO₂ surface doping strategy is introduced to degenerately dope the S/D regions of the FETs and drastically reduce the metal contact resistance, meanwhile revealing intrinsic transport properties of the channel. Along with the previously demonstrated MoS₂ single layer transistor, the results encourage further investigation of layered semiconductors, especially the transition metal dichalcogenide family, for future high performance electronics. As emphasized in this work, surface doping is a necessity for obtaining high performance ML-FETs, and in this regard exploration of other dopant species for both n- and p-doping is needed in the future.

Acknowledgements

This work was funded by NSF E3S Center and FCRP/MSD. The materials characterization part of this work was partially supported by the Director, Office of Science, Office of Basic Energy Sciences, and Division of Materials Sciences and Engineering of the U.S. Department of Energy under Contract No. De-Ac02-05Ch11231 and the Electronic Materials (E-Mat) program. A.J. acknowledges a Sloan Research Fellowship, NSF CAREER Award, and support from the World Class University program at Sunchon National University.

SUPPORTING INFORMATION

Reversibility of NO₂ doping; optical microscope images of a top-gated ML-FET. This material is available free of charge via the Internet at <http://pubs.acs.org>.

Figure Captions

Figure 1. Single layered WSe₂ on a Si/SiO₂ substrate. **a**, Optical microscope image of a single layered WSe₂ (light orange flake) on a Si substrate with 270 nm SiO₂. **b**, AFM image of a single layered WSe₂ on Si/SiO₂. **c**, Height profile of a line scan (as indicated by the dashed line in Fig. 1b) across the single layered WSe₂-SiO₂ boundary.

Figure 2. Back-gated WSe₂ FETs with different metal contacts. **a**, I_{DS} - V_{GS} characteristics of Pd (red curve) and Ti (black curve) contacted WSe₂ FETs on a Si substrate with 50 nm SiO₂ as the back-gate dielectric. Here WSe₂ is few layered (thickness, ~5 nm). **b**, Qualitative energy band diagrams for Pd (top) and Ti (bottom) contacted WSe₂ FETs in the ON-state, depicting the height of the SBs for hole injection (Φ_{Bp}) at the metal-WSe₂ interfaces.

Figure 3. Chemical *p*-doping of single layered WSe₂ by NO₂. **a**, Cross-sectional schematic of a back-gated WSe₂ ML-FET on Si/SiO₂, with NO₂ molecules being absorbed on both the channel and contacts. **b**, I_{DS} - V_{GS} characteristics of Pd contacted WSe₂ ML-FET before (black curve) and after (red curve) exposure to NO₂.

Figure 4. Top-gated WSe₂ ML-FETs with chemically doped contacts. **a**, Schematic of a top-gated WSe₂ ML-FET, with chemically *p*-doped S/D contacts by NO₂ exposure. Here the top-gate acts as the mask for protecting the active channel from NO₂ doping. **b**, Transfer characteristics of a device with $L \sim 9.4$ μm , before and after NO₂ patterned doping of the S/D contacts. **c**, Extracted effective hole mobility as a function of gate overdrive of the device shown in b at $V_{DS} = -0.05$ V. **d**, Output characteristics of the same device shown in b.

References

1. Taur, Y. *IBM J. Rev & Dev.* **2002**, 46, 213-222.
2. Luisier, M.; Lundstrom, M.; Antoniadis, D. A.; Bokor, J. *IEDM Tech. Dig.* **2011**, 251-254.
3. Chau, R.; Kavalieros, J.; Doyle, B.; Paulsen, N.; Lionberger, D.; Barlage, D.; Arghavani, R.; Roberds, B.; Doczy, M. *IEDM Tech. Dig.* **2001**, 621-624.
4. Liu, M.; Yin, X.; Ulin-Avila, E.; Geng, B.; Zentgraf, T.; Ju, L.; Wang, F.; Zhang, X. *Nature* **2011**, 474, 64-67.
5. Schedin, F.; Geim, a K.; Morozov, S. V.; Hill, E. W.; Blake, P.; Katsnelson, M. I.; Novoselov, K. S. *Nat. Mater.* **2007**, 6, 652-655.
6. Frank, O.; Tsoukleri, G.; Riaz, I.; Papagelis, K.; Parthenios, J.; Ferrari, A. C.; Geim, A. K.; Novoselov, K. S.; Galiotis, C. *Nat. Commun.* **2011**, 2, 255.
7. Britnell, L.; Gorbachev, R. V.; Jalil, R.; Belle, B. D.; Schedin, F.; Mishchenko, A.; Georgiou, T.; Katsnelson, M. I.; Eaves, L.; Morozov, S. V.; Peres, N. M. R.; Leist, J.; Geim, A. K.; Novoselov, K. S.; Ponomarenko, L. A. *Science* **2012**, 335, 947-950.
8. Wang, X.; Ouyang, Y.; Jiao, L.; Wang, H.; Xie, L.; Wu, J.; Guo, J.; Dai, H. *Nat. Nanotech.* **2011**, 6, 563-567.
9. Radisavljevic, B.; Radenovic, A; Brivio, J.; Giacometti, V.; Kis, A. *Nat. Nanotech.* **2011**, 6, 147-150.
10. Upadhyayula, L. C.; Loreski, J. J.; Wold, A.; Giriat, W.; Kershaw, R. *J. Appl. Phys.* **1968**, 39, 4736-4740.
11. Yousefi, G. H. *Mater. Lett.* **1989**, 9, 38-40.
12. Podzorov, V.; Gershenson, M. E.; Kloc, C.; Zeis, R.; Bucher, E. *Appl. Phys. Lett.* **2004**, 84, 3301-3303.
13. Kalikhman, V. L.; Umanskii, Y. S. *Sov. Phys. Usp.* **1973**, 15, 728-740.
14. Kong, J.; Franklin, N. R.; Zhou, C.; Chapline, M. G.; Peng, S.; Cho, K.; Dai, H. *Science* **2000**, 287, 622-625.
15. Chen, W.; Chen, S.; Qi, D. C.; Gao, X. Y.; Wee, A. T. S. *J. Am. Chem. Soc.* **2007**, 129, 10418-10422.

16. Wehling, T. O.; Novoselov, K. S.; Morozov, S. V.; Vdovin, E. E.; Katsnelson, M. I.; Geim, A. K.; Lichtenstein, A. I. *Nano Lett.* **2008**, 8, 173-177.
17. Bartram, M. E.; Windham, R. G.; Koel, B. E. *Surf. Sci.* **1987**, 184, 57-74.
18. He, J.-W.; Memmert, U.; Norton, P. R. *J. Chem. Phys.* **1989**, 90, 5088-5093.
19. Joyce, W. B.; Dixon, R. W. *Appl. Phys. Lett.* **1977**, 31, 354-356.
20. Spah, R.; Lux-steiner, M.; Obergfell, M.; Ucher, E.; Wagner, S. *Appl. Phys. Lett.* **1985**, 47, 871-873.
21. Liu, H.; Ye, P. D. *IEEE Electron Device Lett.* **2012**, 33, 546-548.
22. Liu, H.; Xu, K.; Zhang, X.; Ye, P. D. *Appl. Phys. Lett.* **2012**, 100, 152115.
23. Takei, K.; Madsen, M.; Fang, H.; Kapadia, R.; Chuang, S.; Kim, H. S.; Liu, C.-H.; Plis, E.; Nah, J.; Krishna, S.; Chueh, Y.-L.; Guo, J.; Javey, A. *Nano Lett.* **2012**, 12, 2060-2066.

Figure 1

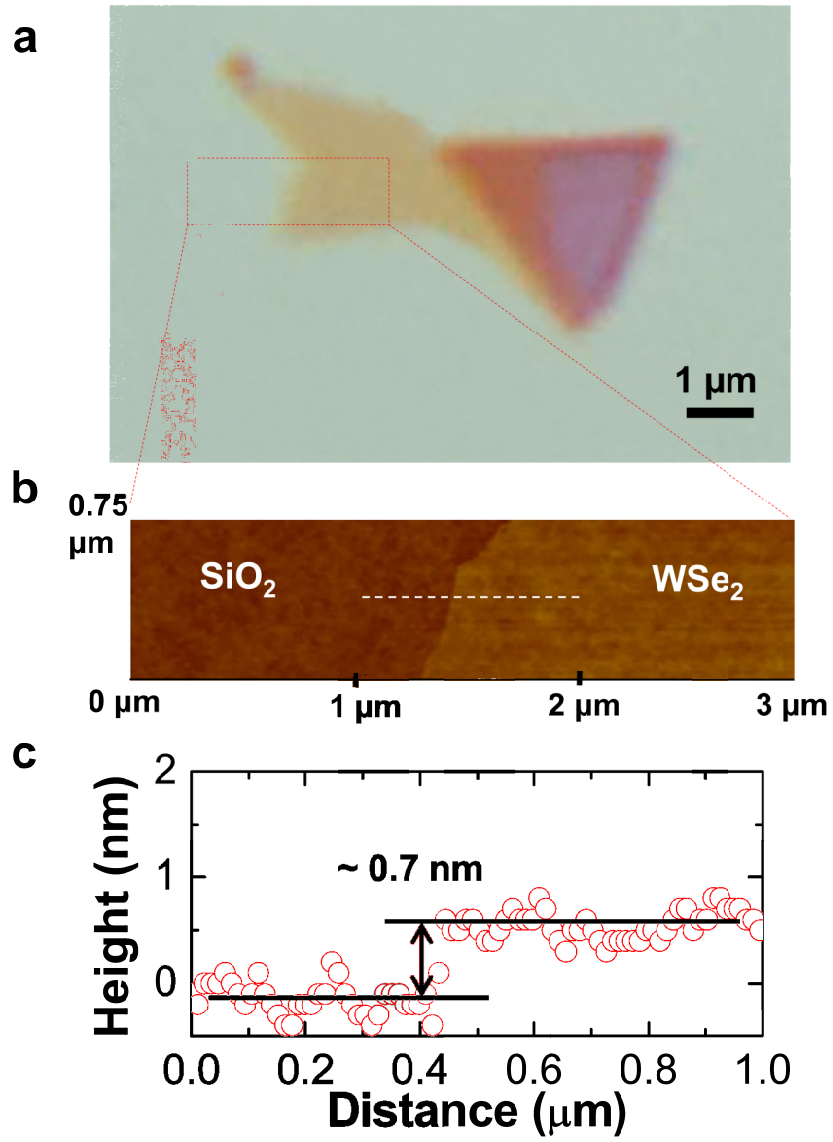


Figure 2

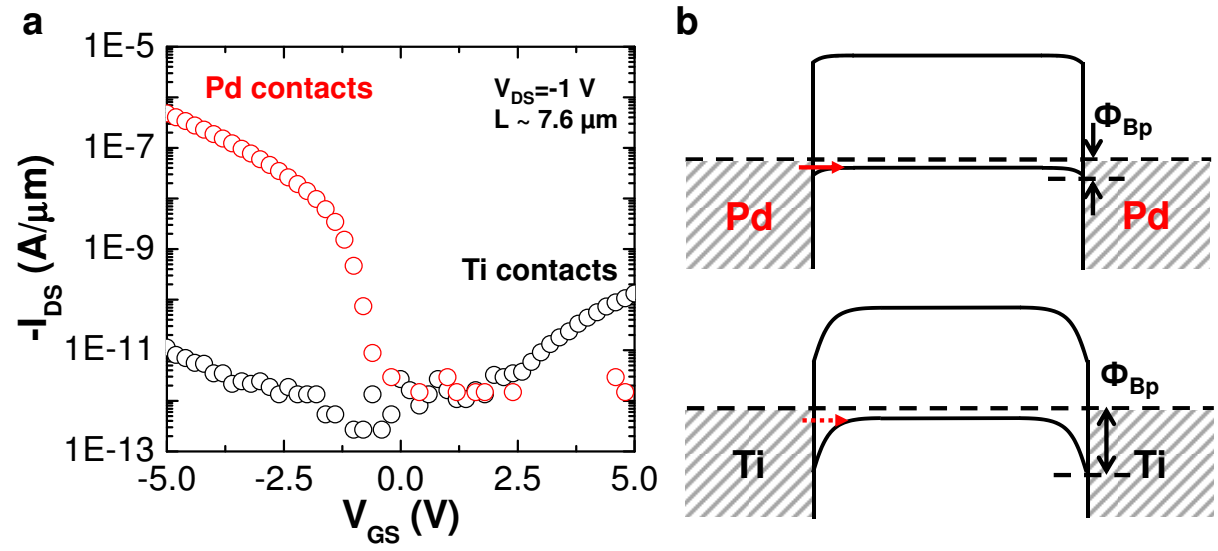


Figure 3

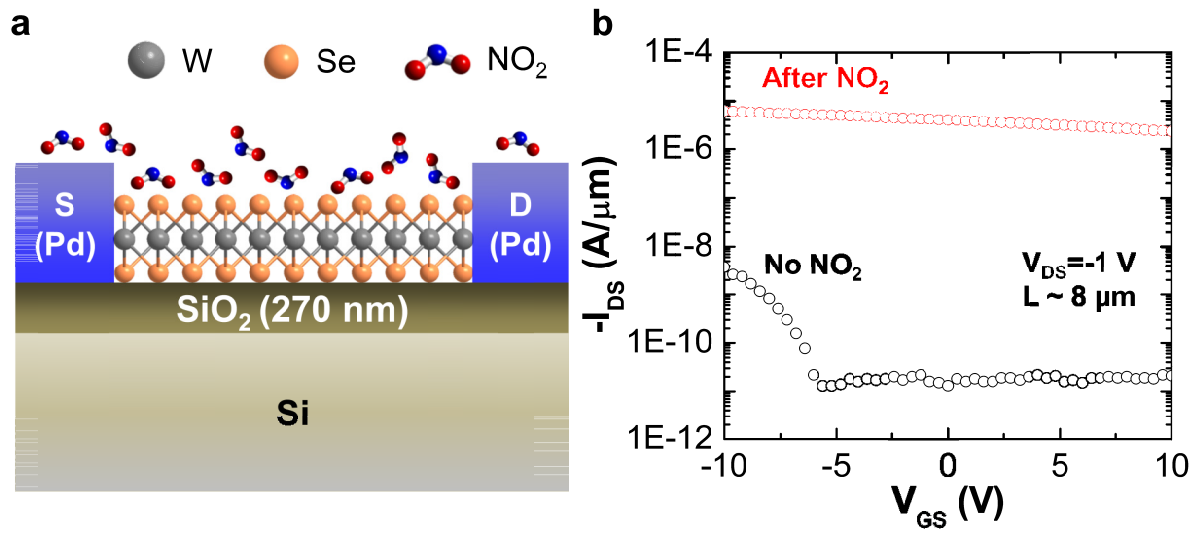


Figure 4

